Supporting Information

Natural Polyphenol-Taurine based Nanoparticles for Oral Ulcer Therapy

Xun Pan, [a,b, †]   Hengjie Zhang, [c, †] Jinling Zhao, [c] Zhipeng Gu, [c] Huixu Xie [a, d *] and Jian Wang [a, b *]

a. State Key Laboratory of Oral Diseases & National Center for Stomatology & National Clinical Research Center for Oral Diseases， West China Hospital of Stomatology, Sichuan University, Chengdu 610041, Sichuan, China

b. Department of Prosthodontics, West China Hospital of Stomatology, Sichuan University, Chengdu 610041, China

c. College of Polymer Science and Engineering, State Key Laboratory of Polymer Materials Engineering, Sichuan University, Chengdu 610065, China.

d. State Key Laboratory of Oral Diseases, National Clinical Research Center for Oral Diseases, Department of Head and Neck Oncology Surgery, West China Hospital of Stomatology, Sichuan University, Chengdu 610041, China.

† The authors contribute equally to this manuscript

* Corresponding author.

E-mail address: xiehuixu@scu.edu.cn (H. Xie); ferowang@hotmail.com(J. Wang)

Address: Sichuan University, No. 14, Section 3, South Peoples Road, Chengdu 610041, China.

Ethics approval statement: All animal experiments were approved by the animal ethics committee of the Sichuan University (WCHSIRB-AT-2025-608)

Table. S1. Component proportions used in PA and PAT NPs preparation

Sample	Protocatechualdehyde (mg)	Taurine (mg)	KIO_3 (mg)	Deionized water (mL)	Acetone (mL)
PA	300	0	465	150	5
PAT	300	270	465	150	5

Table. S2. Primers for Quantitative Real-Time PCR.

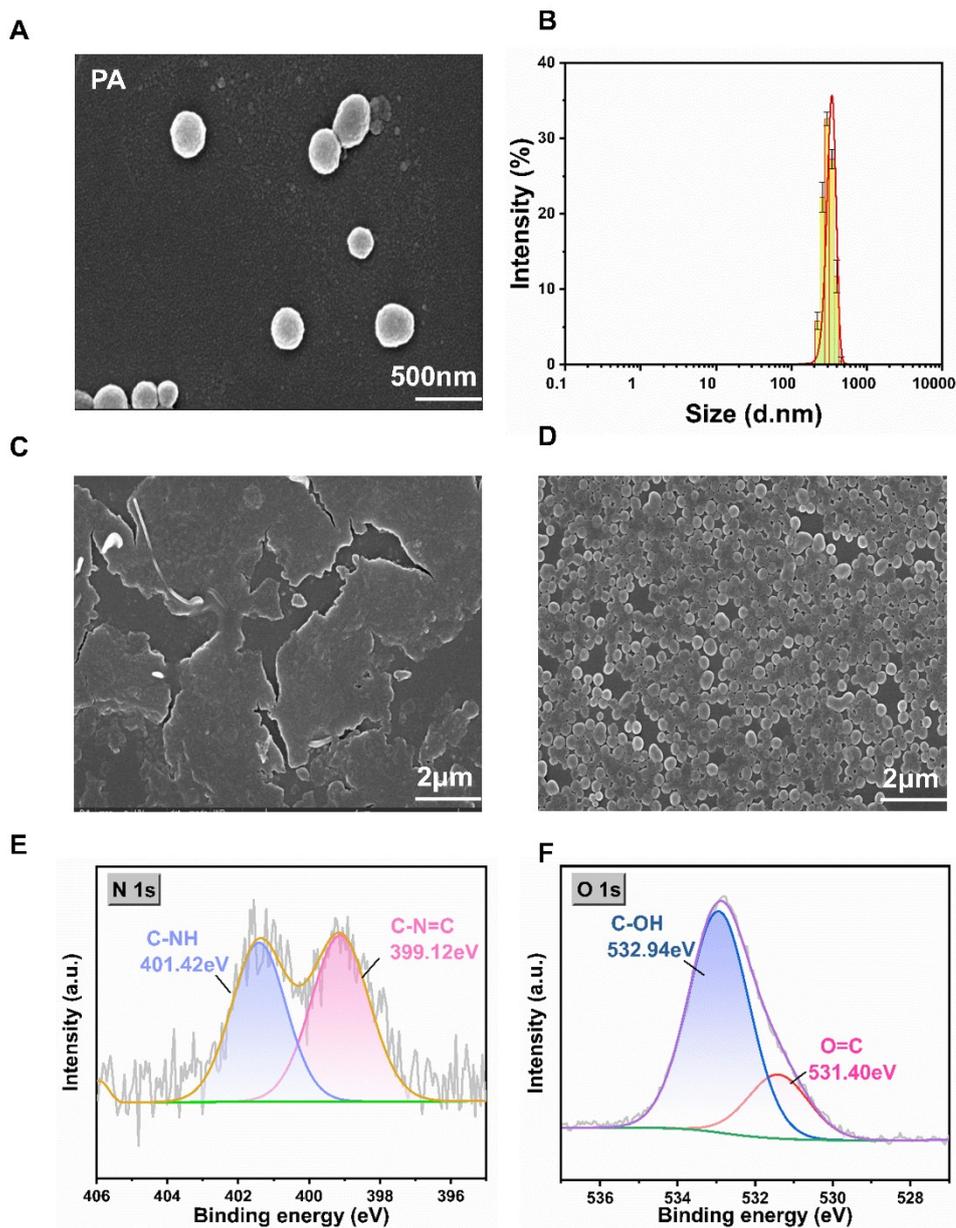| Gene name	Primer	Sequence (5' -3')
GAPDH	Forward	AAGAAGGTGGTGAAGCAGGC
	Reverse	GTCAAAGGTGGAGGAGTGGG
	Forward	GAGCCTTGCCTTGCTGCTCTA
VEGF	Reverse	CACCAGGGTCTCGATTGGATG

Figure S1. Characterization of nanoparticles. (A) Schematic illustration of the preparation process of PA nanoparticles. (B) Hydrodynamic size distribution of PA nanoparticles. (C) Irregular flake-like substances synthesized with a PCA to taurine ratio of 1:1. (D) Spherical nanoparticles synthesized with a PCA to taurine ratio of 1:0.5. (E) N1s spectrum analysis of PAT nanoparticles. (F) O1s spectrum analysis of PAT nanoparticles.
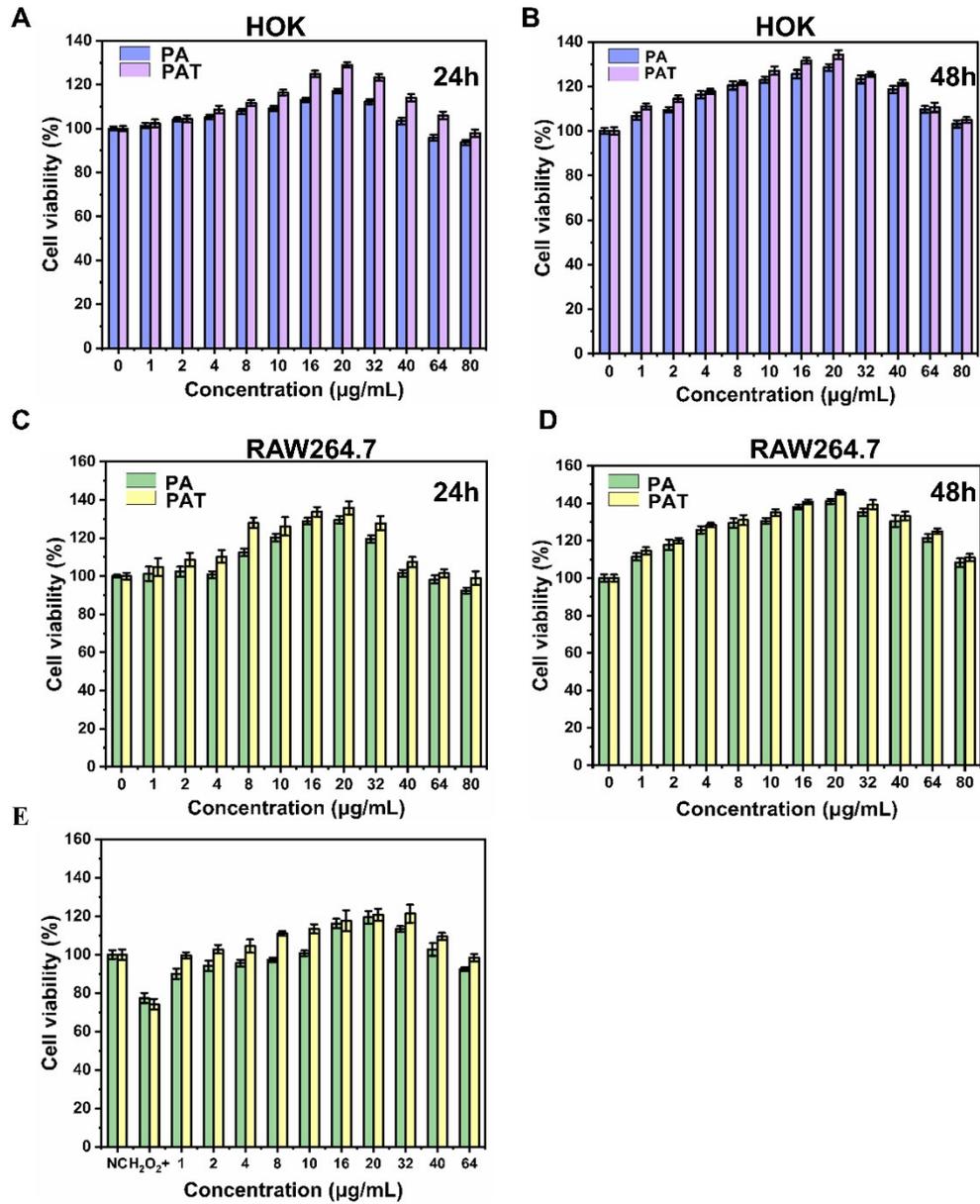
Figure S2. Biocompatibility of nanoparticles. (A) Cell viability of HOK after 24 h. (B) Cell viability of HOK after 48 h.

(C) Cell viability of RAW264.7 after 24 h. (D) Cell viability of RAW264.7 after 48 h. (E) Cell viability of RAW264.7 at

200 mM H_2O_2 after 24 h. (F) Fluorescence images of total reactive oxygen species (ROS) in HOK and RAW264.7 cells
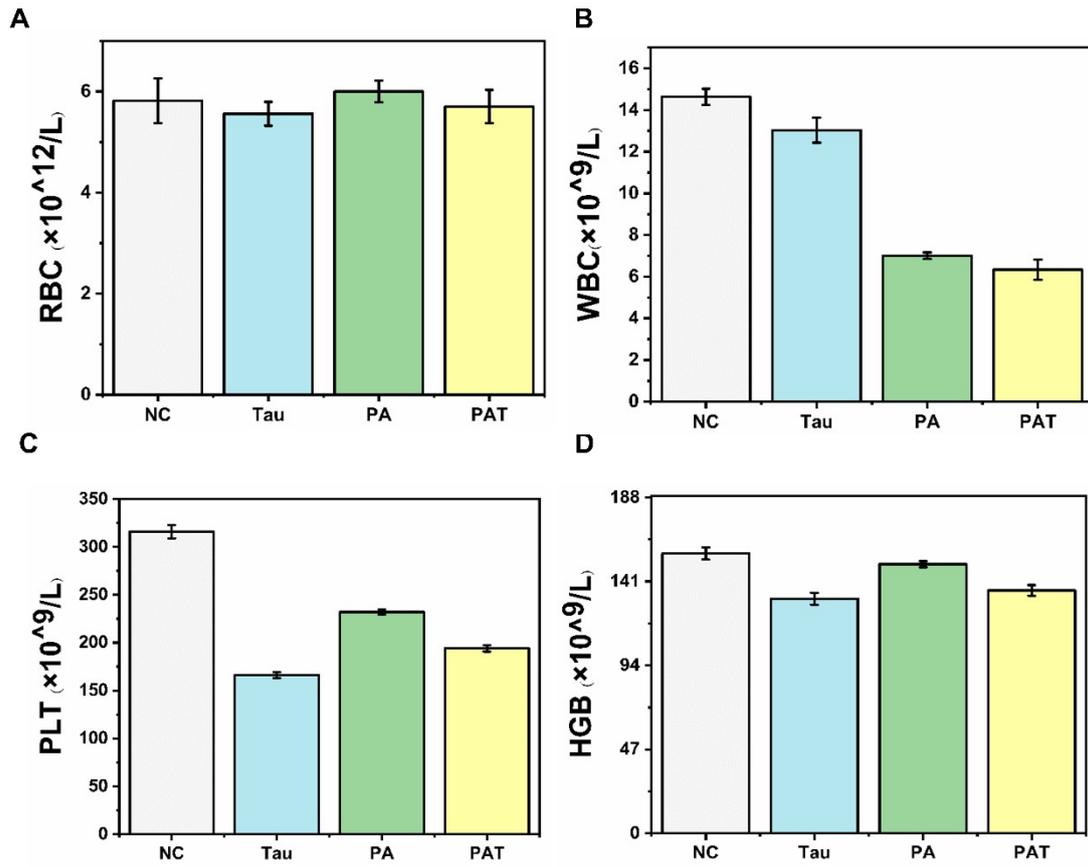
in the NC group.

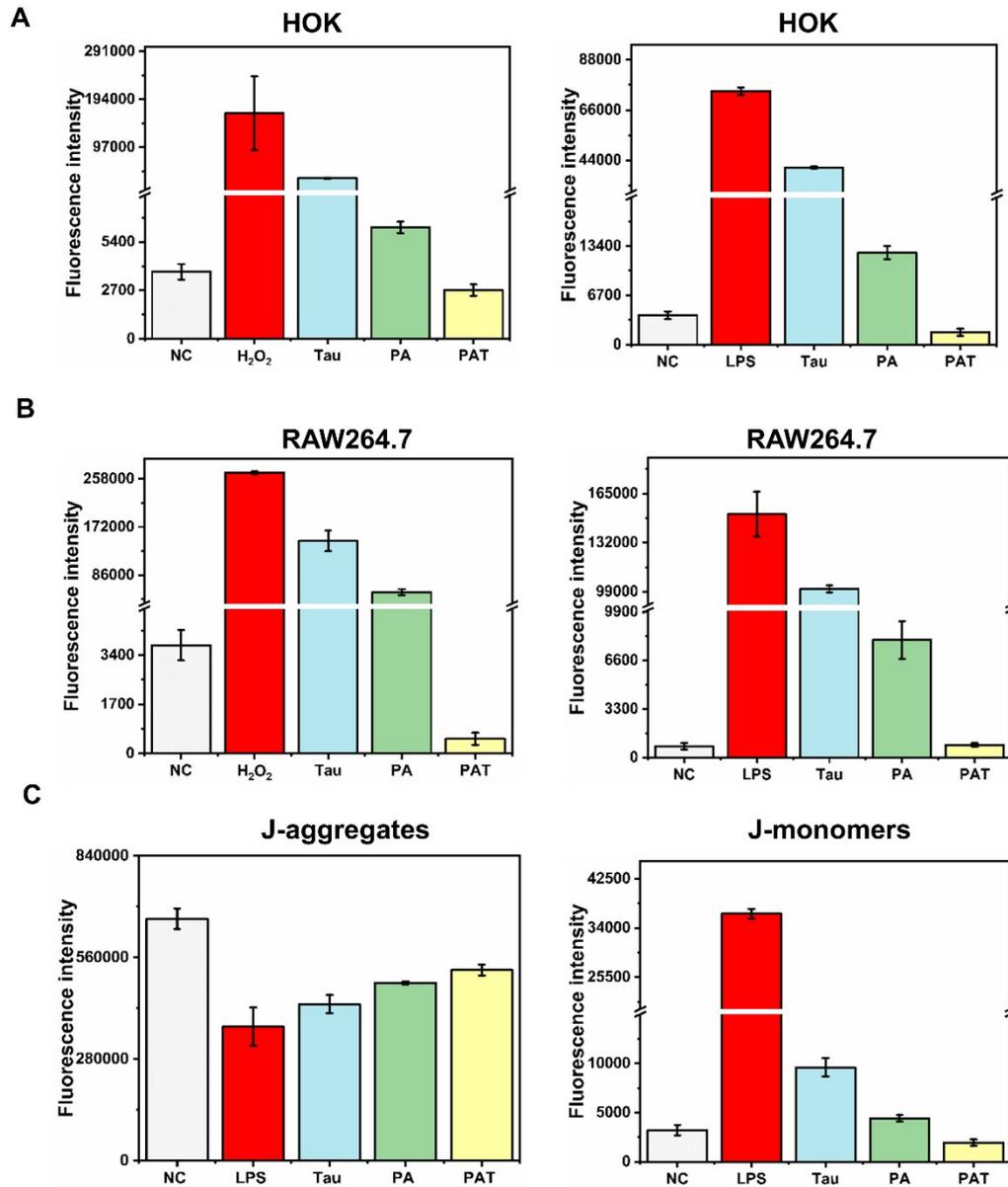**Figure S3. Hematological analysis of SD rats after treatment in each group.**

Figure S4. Quantitative fluorescence analysis. (A) Statistical analysis of the relative mean fluorescence intensity of total reactive oxygen species (ROS) in HOK cells under LPS induction (left) and H_2O_2 induction (right). (B) Statistical analysis of the relative mean fluorescence intensity of total reactive oxygen species (ROS) in RAW264.7 cells under LPS induction (left) and H_2O_2 induction (right). (C) Statistical analysis of the relative mean fluorescence intensity of mitochondrial membrane potential in each group under LPS induction.
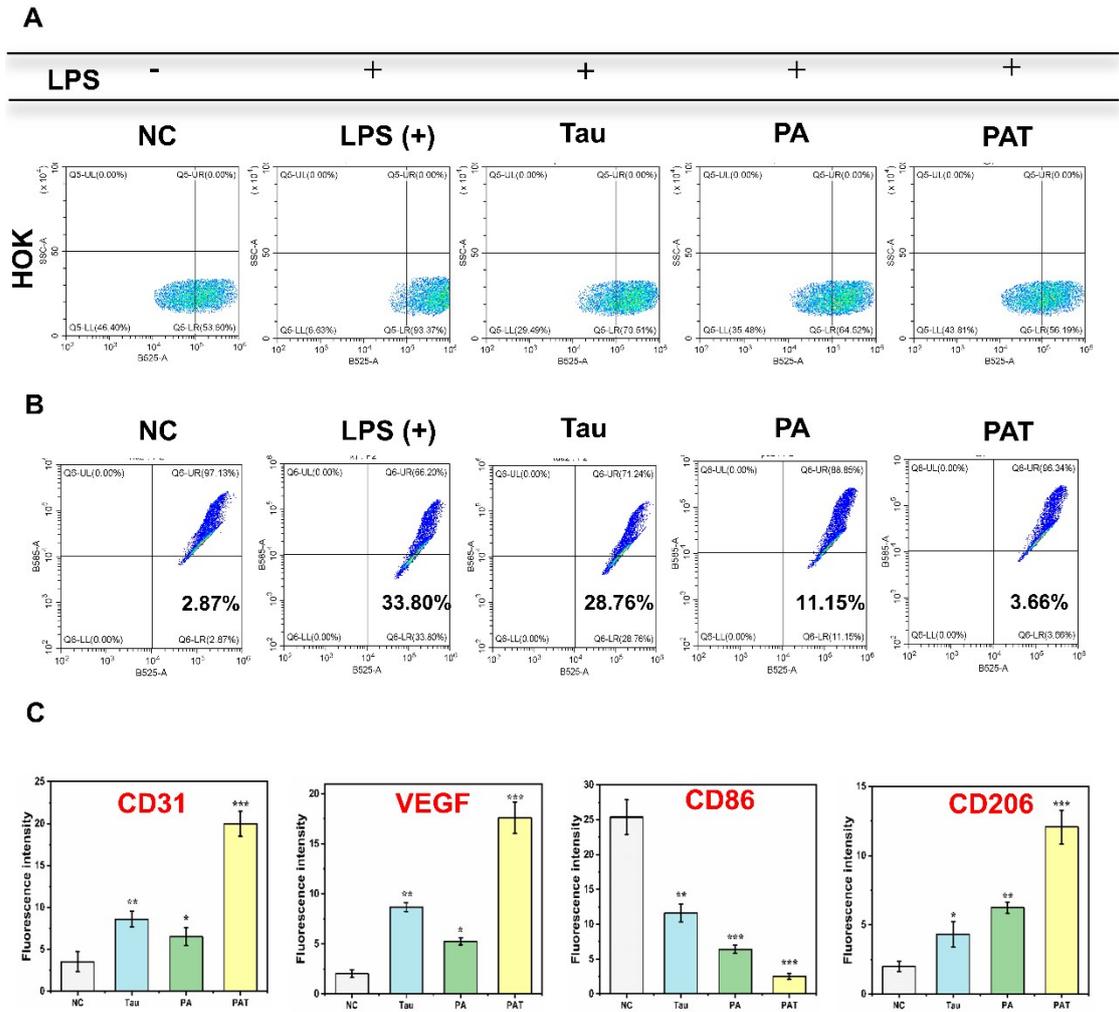
Figure S5. (A) Flow cytometry analysis of ROS scavenging in HOK cells under LPS induction in each group. (B) Flow cytometry analysis of mitochondrial membrane potential changes in RAW264.7 cells under LPS induction in each group. (C) Statistical analysis of relative mean fluorescence intensity of CD31, VEGF, CD86, and CD206 (based on immunofluorescence staining images).
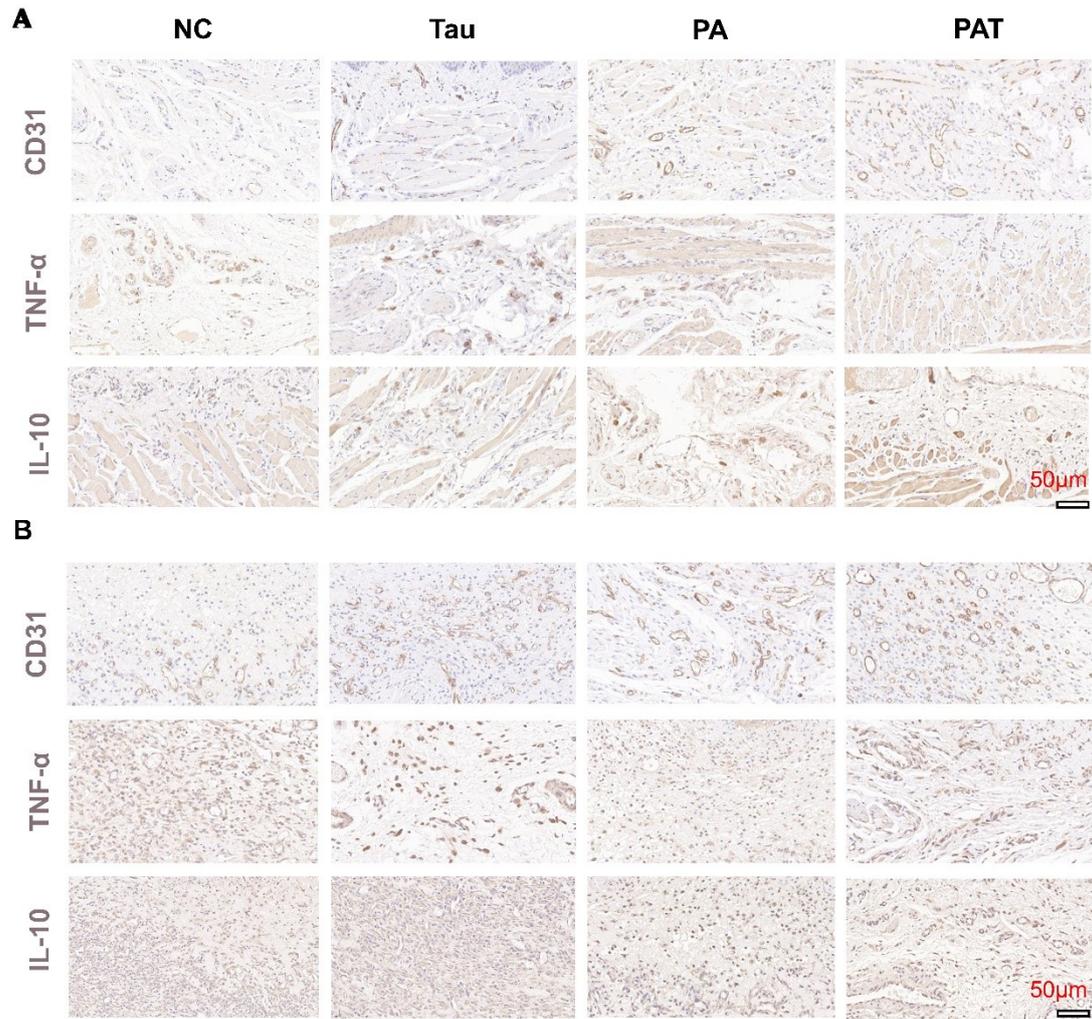
Figure S6. (A) Immunohistochemical staining results for CD31, TNF-α, and IL-10 in tongue ulcer tissues from different groups on day 4. (B) Immunohistochemical staining results for CD31, TNF-α, and IL-10 in gingival ulcer tissues from different groups on day 6.
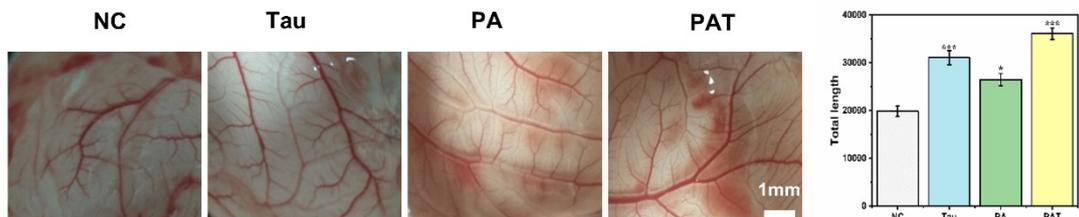

Figure S7. Evaluation of the angiogenic capacity of PAT using the CAM model.
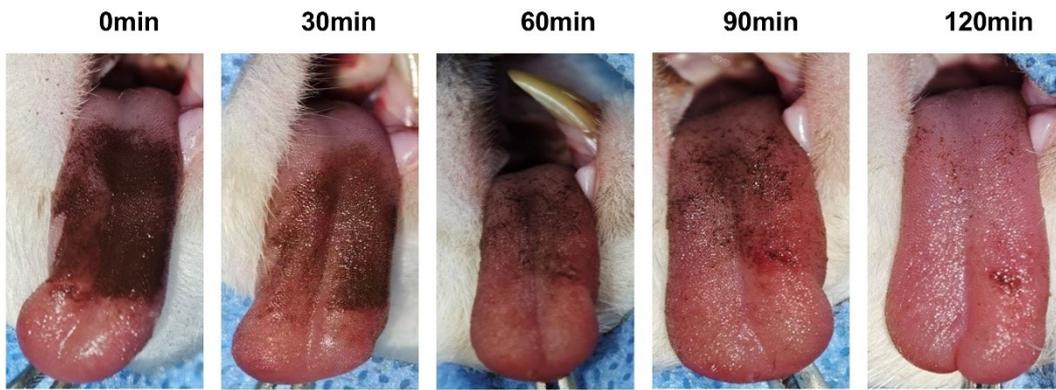
Figure S8. The mucosal retention of PAT was evaluated at various time intervals following administration.